Measurement of Tritium Distribution in Nickel and Vanadium by Means of A Combined Technique of An Imaging Plate and Thin Absorbers

Hiroko YOSHIDA-OHUCHI, Yuji HATANO[1)], Akram MOHAMMADI[2)] and Takao KAWANO[3)]

Radioisotope Research and Education Center, Graduate School of Pharmaceutical Science, Tohoku University, Sendai 980-8578, Japan

[1)]Hydrogen Isotope Research Center, University of Toyama, Toyama 930-8555, Japan

[2)]Radiation Research Center, Shiraz University, Shiraz 85111-71946, Iran

[3)]National Institute for Fusion Science, Toki-city 509-5292, Japan

(Received: 10 May 2012 / Accepted: 21 October 2012)

A combined technique of an imaging plate (IP) and thin absorbers was applied to tritium in nickel and vanadium specimens using copper, aluminum, and gold foil as the absorber. Copper and aluminum foil are used as a K-edge filter with X-ray absorption at 9.0 keV and 1.56 keV, respectively. Gold has L-edges X-ray absorption at around 13 keV. With this technique, photostimulated luminescence (PSL) decay curves are obtained by changing absorber's thickness. In the nickel specimen, the difference in PSL decay curves between for the copper and gold absorber was clearly observed 20 days after loading, however, all curves became similar single pattern after 388 days. The same curve pattern was obtained in vanadium for all absorbers. The cross section images and depth profiles, which were taken at 468 days and 3.9 years after loading for the nickel and vanadium specimen, respectively, show no significant inclination of tritium concentration for both specimens. These results indicate that uniform tritium distribution in the specimen provides the similar single PSL decay curves pattern for the copper or aluminum and gold absorber.

Keywords: tritium, imaging plate, thin absorber, bremsstrahlung X-rays, depth distribution, non-destructive measurement

1. Introduction

Non-destructive and quantitative measurement of the amount of tritium retained on/in plasma-facing materials (PFMs) of magnetic fusion devices are of great importance for the control of fuel particles and to ensure safety for maintenance work and waste processing of PFMs in fusion systems. The tritium imaging plate (IP) technique for detecting beta particles is useful to non-destructively determine the surface tritium distribution on PFMs [1-5]. An IP made of europium-doped BaFBr(I), a photostimulated luminescence (PSL) material, is a two-dimensional radiation sensor. This IP has many excellent properties making it suitable for this purpose, including high sensitivity, wide dynamic range over five orders of magnitude, a high degree of spatial resolution, and reusability by exposing the IP to visible light between uses [6].

Tritium emits beta particles with a maximum energy of 18.6 keV, with an average of 5.7 keV. These have a range of about several micrometers in graphite, and hence the IP technique is sensitive to tritium up to a depth of a few microns. In order to obtain tritium distribution in regions deeper than the escape depth of beta rays from tritium, we have been developing a combined technique of an imaging plate (IP) and thin absorbers using the bremsstrahlung X-rays generated by the interaction between the beta particles from tritium and matter [7].

In this study, the combined technique of the IP and thin absorbers was applied to tritium in nickel and vanadium specimens using copper, gold, and aluminum foil as the absorber. Copper and aluminum foil are used as a K-edge filter with X-ray absorption at 9.0 keV and 1.56 keV, respectively. Gold has L-edges X-ray absorption at around 13 keV [7].

2. Experimental

Tritium was introduced into sheet type specimens (1.5 x 1.5 x 0.05 cm^3) of nickel by gas absorption method at 673 K on 24 Dec 2010 in the manner described in the previous paper [8]. Specimens were loaded with deuterium containing 17% tritium. For vanadium specimen (4.8 x 1.0 x 0.05 cm^3), tritium was introduced by the same method at 673 K on 27 May 2008 [9]. The tritium concentration in the specimen was controlled to be 1.0 appm; the total concentration of tritium and deuterium was 200 appm. Then all specimens were kept at room temperature.

The initial distribution of tritium in the nickel specimen was examined by β-ray induced X-ray spectroscopy (BIXS) under Ar atmosphere in the manner described in the previous paper [10]. Tritium distribution

author's e-mail: hiroko@m.tohoku.ac.jp

was measured twice, 20 and 388 days after tritium loading for the nickel specimen and 3.5 years for the vanadium specimen, respectively by the combined technique of a BAS-MS type-IP (Fujifilm Co., Ltd.) and absorbers. At the same time, tritium in the surface regions was measured by using a BAS-TR type-IP (Fujifilm Co., Ltd.). The BAS-MS type-IP was used to detect bremsstrahlung X-rays from tritium. This IP consists of a 9-μm-thick polyethyleneterephthalate protective film and a 115-μm-thick photostimulable phosphor layer affixed to a 12-μm-thick plastic back layer and a 190-μm-thick polyethyleneterephthalate base layer [11]. It has a high sensitivity to photons. The BAS-MS type-IP can detect bremsstrahlung X-rays, but not the beta particles emitted from tritium because of its thick protective film. The BAS-TR type-IP lacking a protective surface layer was developed for detection of the beta particles from tritium. This IP consists of a 50-μm-thick photostimulable phosphor layer affixed to a 250-μm-thick base layer.

The BAS-MS type-IP was irradiated with bremsstrahlung X-rays by placing the specimen directly on the IP or with inserting absorbers for 1 h. To avoid contamination of the IP during irradiation, each specimen was sandwiched with a quite thin 1.2-μm-thick film. The schematic diagram of the irradiation setup is shown in Fig. 1. During irradiation, the IP was kept inside a refrigerator with temperature controlled to 4°C, in order to decrease the fading effect, although the BAS-MS-type IP shows good fading characteristics at room temperature [12]. The IP was kept for 20 min after irradiation and then read to avoid fading effects caused by the short half-life component. A model FLA7000 IP reader (Fujifilm Co., Ltd.) was used with a spatial resolution of 100 μm and 8 bits of digital resolution dpi, followed by an image analysis with the Multi Gauge (ver.3.2). For each irradiation, the IP was simultaneously irradiated with a ^{137}Cs disk-shaped gamma-ray source and measured PSL values obtained from the specimen were corrected by that obtained by the ^{137}Cs source to minimize errors induced by the readout system and the procedure. To detect tritium in the surface regions, the BAS-TR type-IP was irradiated with the beta particles by placing the specimen directly on the IP without using the film for 20 min.

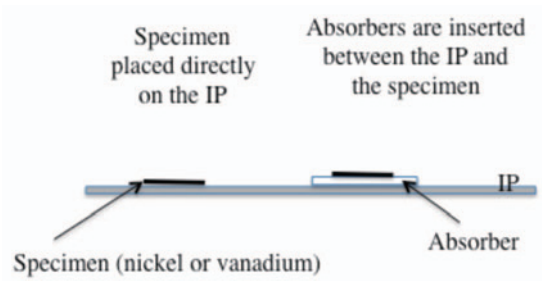

Fig.1 Schematic diagram of the irradiation setup.

3. Results and Discussion

Fig.2 shows X-ray spectrum from the nickel specimen containing tritium. A sharp intense peak of Ar Kα X-rays is at around 3 keV. Another sharp peak at 7.48 keV can be assigned to Ni Kα X-rays. It should be noted that relatively small intensity of Ni Kα peak in comparison with Ar Kα peak. Ar Kα X-rays are induced by tritium in shallow surface region, while Ni Kα X-rays are induced mainly by tritium in the bulk. The spectrum in Fig.2 indicates that tritium is concentrated in the surface regions, which is consistent with the result shown in the previous paper [8].

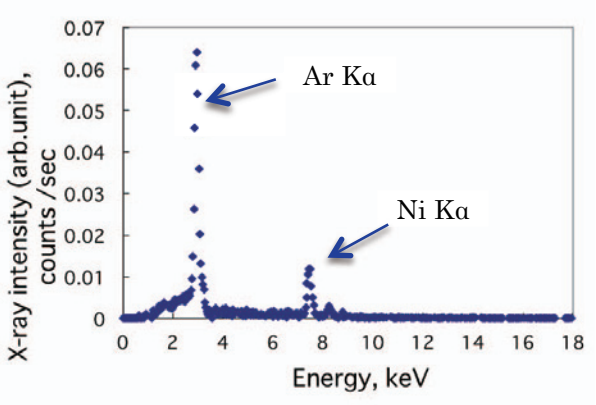

Fig.2 Characteristic BIXS spectrum of a tritium-containing nickel specimen.

Fig.3(a) shows a BAS-TR image for the nickel specimen taken at 20 days after loading, describing tritium two-dimensional distribution in the surface region. The PSL intensity along the line A and B are shown in Fig.3(b), respectively, expressing flat distributions along both lines at the same PSL intensity level except the edge. The

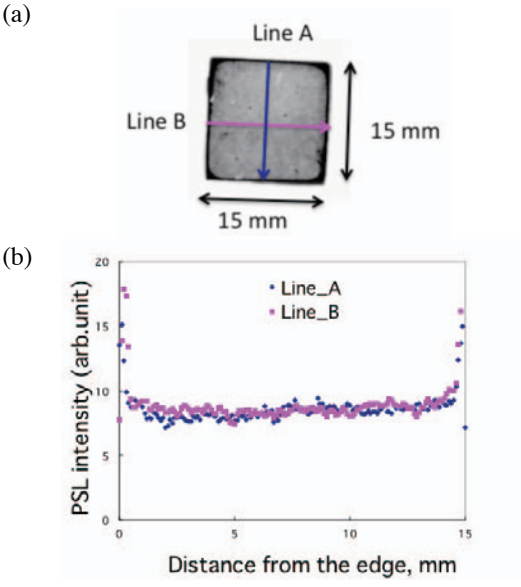

Fig.3 (a) BAS-TR image for the nickel specimen taken at 20 days after loading. (b) PSL intensity along the line A and B.

average PSL intensity per arbitrary unit is 8.4 on the flat curves. The image taken at 388 days after loading was exact the same one with that at 20 days in Fig.3(a) but with a decrease of 16.3% in the average PSL intensity.

Fig.4(a) shows BAS-MS images for the nickel specimen taken at 20 days after loading when the thickness of each absorber varied, exhibiting quite different images compared with the BAS-TR image in Fig.3(a). Each PSL value in the area of 85 mm^2 at the center of the specimen was obtained, and then PSL decay curve was obtained by normalizing the measured PSL values to the PSL value without absorber. Fig.4(b) shows PSL decay curves as a function of the effective thickness for three absorbers. The effective thickness, $\mu \cdot t$, which normalizes the thickness of each absorber by $1/\mu$, was obtained by the following equation:

$$\mu \cdot t = (\mu / \rho) \cdot \rho \cdot t \qquad (1)$$

where μ/ρ is the mass attenuation coefficient (cm^2/g) at K or L-edge X-ray absorption for copper and aluminum absorbers and gold absorber, respectively [13], ρ density (g/cm^3), and t the thickness of absorbers (cm). The scale of the effective thickness for aluminum absorber is expressed as 1/10 in Fig.4(b). When X-rays energy spectrum distribution spreads over some energies, the slope of PSL decay curve is expected to change as the thickness of the absorber increases.

(a)

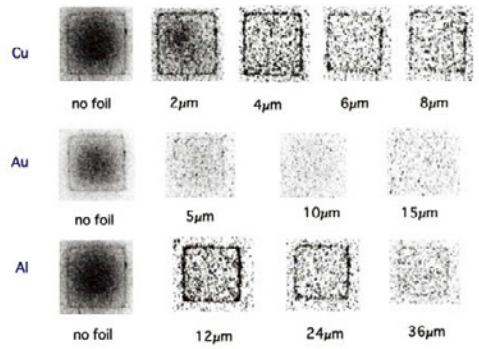

(b)

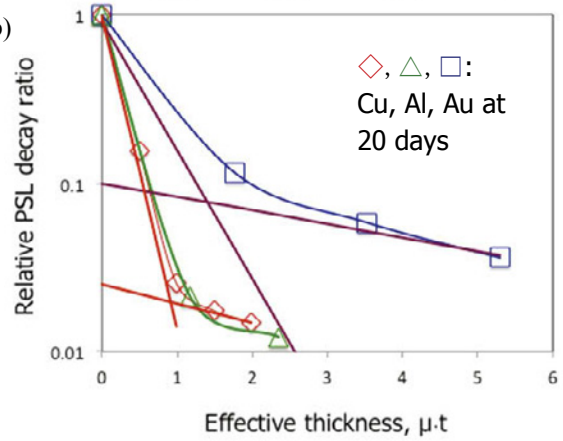

Fig.4 (a) BAS-MS type-IP images for the nickel specimen taken at 20 days after loading when the thickness of each absorber varied. (b) PSL decay curves as a function of the effective thickness for three absorbers. The scale of the effective thickness for aluminum absorber is expressed as 1/10. PSL decay curves for copper and aluminum absorbers are shown as ◇, △ respectively and that for gold is shown as □. Solid lines express two components of PSL decay curves for copper and gold absorbers .

PSL decay curves pattern for copper and aluminum absorbers (shown as ◇, △ respectively) are similar, while that for gold (shown as □□□is quite different from others. In the previous paper [7], we described the principle of the combined technique of the IP and absorbers and how each absorber works when the bremsstrahlung energy spectrum distribution changes as tritium migrates into matter, that is, PSL values derived from the lower energy range rapidly decrease as the copper and aluminum absorber thickness increase. On the other hand, the gold absorber works oppositely, rapidly reducing PSL derived from the higher energy range. Thus, PSL decay curve consists of two components, with fast and slow rates of decay, and they can be expressed in the following equation [7]:

$$f(x) = a \cdot e^{-\mu 1 x} + b \cdot e^{-\mu 2 x} \qquad (2)$$

where a and b are the relative ratio of two components, μ_1 and μ_2 penetrating coefficient of each component, and x is the thickness of the absorber. Two components of PSL decay curves for copper and gold absorbers are shown as solid lines in Fig.4(b). The differences in relative ratio of two components and penetrating coefficient of each component between two PSL decay patterns for copper and gold absorbers are summarized in Table 1. The relative ratio of two components, a and b is considered to indicate the ratio of higher and lower energy bremsstrahlung X-rays in the bremsstrahlung energy spectrum distribution [7].

Table 1 Differences in relative ratio of two components, a and b and penetrating coefficient of each component, μ_1 and μ_2 between two PSL decay patterns for copper and gold absorbers.

Absorber	a	b	μ_1	μ_2
Copper	0.98	0.020	4.0	0.15
Gold	0.90	0.10	1.7	0.19

The same measurements were repeated at 388 days after loading. BAS-MS images show a large decrease of 98% in PSL intensity in comparison with that at 20 days, which can be caused by chronic release from nickel under ambient air at room temperature [8]. PSL decay curves as a function of the effective thickness for three absorbers taken at 388 days are shown in Fig.5(a) and all PSL decay curves at 20 and 388 days after loading are summarized in Fig.5(b). It should be noted that Fig.5(a) shows no differences in the PSL decay curves pattern for three absorbers and these curves became close and similar to the

curve for the gold absorber at 20 days in Fig.5(b). The change in the PSL decay curves for copper and aluminum absorbers between 20 and 388 days can be explained by the diffusion process. Diffusion coefficient (D) at 293 K is calculated for tritium through nickel to be 2.5 x 10^{-14} (m^2/s) using literature values [14]. At 20 days after loading, tritium concentration is considered to distribute with a gradient as Dt/l^2 is calculated to be 0.3 (l=0.25 mm) and then a diffusion process ends at 388 days as Dt/l^2 is calculated to be 13 (>> 1.0) [15]. Based on the preliminary results obtained by simulating the bremsstrahlung energy spectrum with Monte Carlo N-Particle Transport Code (MCNP), the spectrum distribution spreads over lower to higher range at 20 days because tritium concentration distributes with the gradient, and the spectrum distribution changes with time, shifting its peak to higher energy with a decrease of lower energy bremsstrahlung X-rays because tritium concentration distribution loses the gradient as the diffusion process proceeds and the uniform tritium distribution is formed in the specimen after 388 days. The relative ratio, a, the component with fast rate of decay for the copper absorber at 388 days was determined as 0.72, which became smaller than that at 20 days (0.98 in Table 1), indicating PSL derived from the lower energy range decreased with time. This result is consistent with the assumed theory. On the contrary, the PSL decay curve for the gold absorber does not seem to have changed with time. This is because PSL derived from the higher energy range does not decrease through the diffusion process. Then, at a result, all PSL decay curves for three absorbers are considered to become similar at 388 days.

The combined technique of the IP and thin absorbers was applied to tritium in the vanadium specimen and PSL decay curves as a function of the effective thickness for three absorbers were obtained (shown in Fig.6), expressing the same pattern with those in the nickel specimen for three absorbers at 388 days.

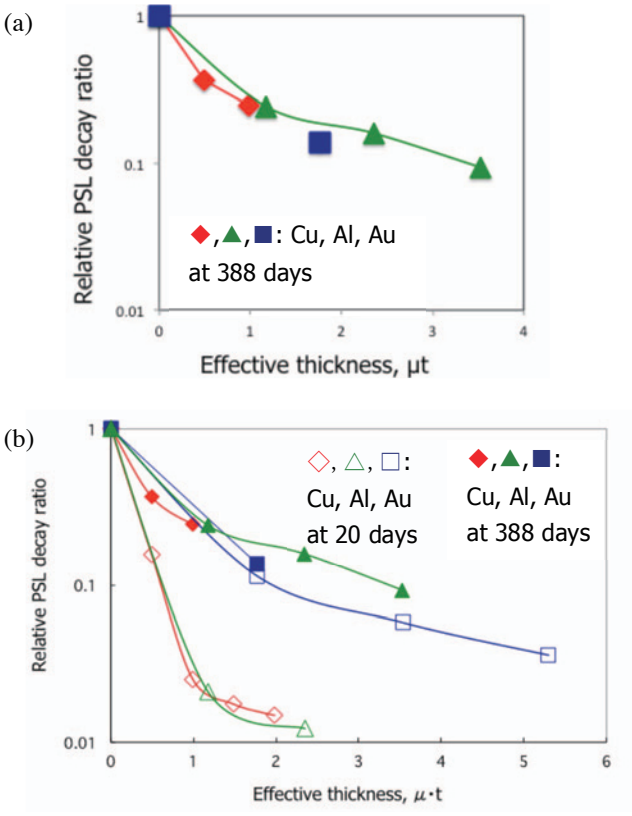

Fig.5 (a) PSL decay curves for the nickel specimen as a function of the effective thickness for three absorbers taken at 388 days after loading. (b) All PSL decay curves at 20 and 388 days after loading. Curves for copper, aluminum, and gold absorbers are shown as ♦,▲, and ■ at 388 days and ◇, △, and □ at 20 days, respectively. The scale of the effective thickness for aluminum absorber is expressed as 1/10 in both figures.

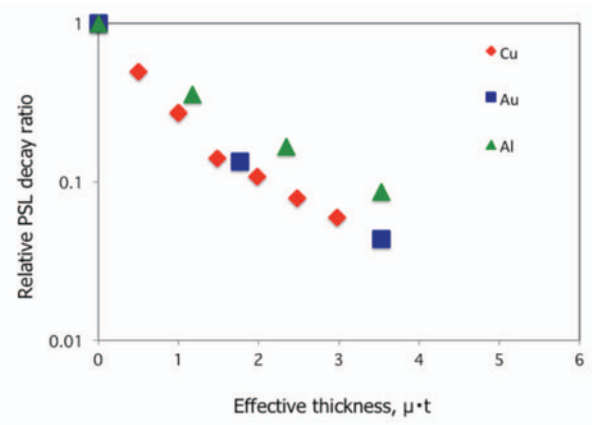

Fig.6 PSL decay curves as a function of the effective thickness for the vanadium specimen. The scale of the effective thickness for aluminum absorber is expressed as 1/10.

In order to obtain tritium distributions in the nickel and vanadium specimen, cross section images and depth profiles were obtained by autoradiography. They were taken at 468 days and 3.9 years after loading for the nickel and vanadium specimen, respectively. Both specimens were cut through the middle and the BAS-TR type-IP was irradiated by contacting the cross section of the specimen directly on the IP for 47 h. To avoid high concentrated tritium on the nickel surface, the side of the cross section was covered with tape during irradiation. The cross section images and depth profiles so obtained are shown in Fig.7(a) and (b) for the nickel and vanadium specimen, respectively. Through the cross section, no significant inclination of tritium concentration was observed in both images and depth profiles. The observation for the nickel specimen in Fig.7(a) can be explained by the diffusion

process. The process ended at 388 days as mentioned above and then tritium distribution is supposed to be uniform in the specimen except high concentrated tritium on the surface. For the vanadium specimen, the diffusivity of tritium is much larger than that in the nickel [9] and the diffusion process ended at the time when autoradiography was obtained, resulting in uniform tritium distribution in the vanadium specimen. These observations for two specimens indicate that uniform tritium distribution in the specimen provides the similar single PSL decay curves pattern for the copper or aluminum and gold absorber.

From comprehensive results, this technique can be used usefully to observe tritium depth distribution in matter nondestructively. Further investigation should be needed for the analysis about the relationship between tritium distribution in the specimen and PSL decay curves pattern by simulating the bremsstrahlung energy spectrum with MCNP Code.

(a)

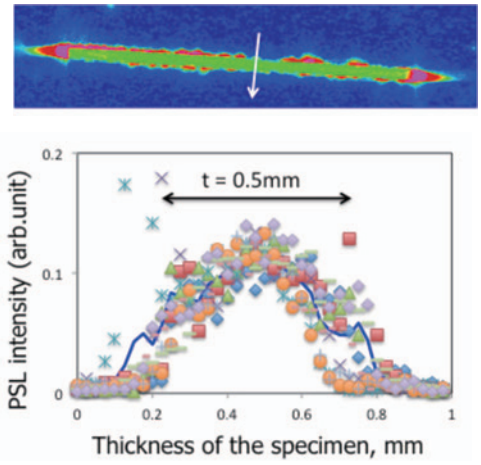

(b)

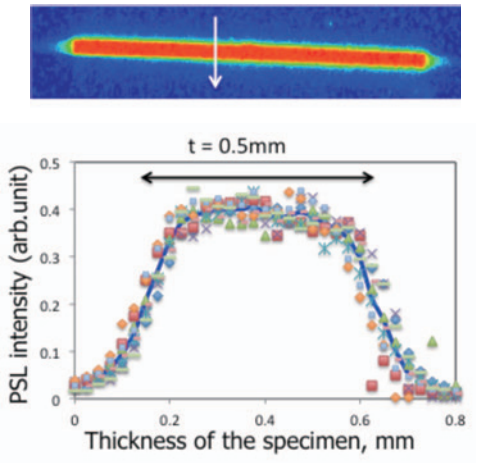

Fig.7 BAS-TR autoradiography cross section images and depth profiles for the nickel (a) and vanadium (b) specimen, respectively. In each figure, the average profile obtained from 10 profiles is shown in a line.

Acknowledgments

This study has been supported in part by KAKENHI on Priority Areas, 476, Tritium for Fusion, from MEXT, Japan, and the National Institute for Fusion Science under the Joint Work contract #NIFS12KUHR017, as a part of Bilateral Collaboration Project with University of Toyama. The author is grateful to Professor Yasuhiro Kondo of Ishinomaki Senshu University for his advice.

[1] T. Tanabe *et al.*, Fus. Eng. and Des. **54**, 147 (2001).
[2] K. Miyasaka *et al.*, J. Nucl. Mater. **307-311**, 1441 (2002).
[3] K. Masaki *et al.*, J. Nucl. Mater. **313-316**, 514 (2003).
[4] T. Tanabe *et al.*, J. Nucl. Mater. **313-316**, 478 (2003).
[5] K. Sugiyama *et al.*, J. Nucl. Mater. **313-316**, 507 (2003).
[6] J. Miyahara *et al.*, Nucl. Instr. and. Meth. **A 246**, 572 (1986) .
[7] H. Ohuchi-Yoshida *et al.*, Fus. Eng. and Des. **87**, 423 (2012).
[8] M. Saito *et al.*, Fus. Sci. Technol. **60**, 1459 (2011)
[9] Y.Hatano *et al.*, Proceedings of 2nd Japan-China Workshop on Blanket and Tritium Technology 100 (2008)
[10] Y.Torikai *et al.*, J. Nucl. Mater. **363-365**, 462 (2007)
[11] Fuji Film Co., Ltd. Homepage, http://www.fujifilm.com/products/life_science_systems/science_imaging/imaging_plate/faq/
[12] H. Ohuchi *et al.*, Nucl. Instr. and. Meth. **A 490**, 573 (2002).
[13] NIST Homepage, http://physics.nist.gov/PhysRefData/XrayMassCoef/tab3.html.
[14] F. Reiter *et al.*, EUR 15217 EN (1993).
[15] J.Crank, The mathematics on diffusion 2nd edition (Oxford university press, New York, 1975) p.50.